Published in final edited form as:

Muscle Nerve. 2017 April ; 55(4): 544–554. doi:10.1002/mus.25273.

CHRONIC PERIPHERAL NERVE COMPRESSION DISRUPTS PARANODAL AXOGLIAL JUNCTIONS

Yoshinori Otani, PhD[1,*], **Leonid M. Yermakov, BS**[1], **Jeffrey L. Dupree, PhD**[2], and **Keiichiro Susuki, MD, PhD**[1]

[1]Department of Neuroscience, Cell Biology, and Physiology, Boonshoft School of Medicine, Wright State University, Dayton, Ohio 45435, USA

[2]Department of Anatomy and Neurobiology, Virginia Commonwealth University, Richmond, Virginia 23298, USA

Abstract

Introduction—Peripheral nerves are often exposed to mechanical stress leading to compression neuropathies. The pathophysiology underlying nerve dysfunction by chronic compression is largely unknown.

Methods—We analyzed molecular organization and fine structures at and near nodes of Ranvier in a compression neuropathy model in which a silastic tube was placed around the mouse sciatic nerve.

Results—Immunofluorescence study showed that clusters of cell adhesion complex forming paranodal axoglial junctions were dispersed with frequent overlap with juxtaparanodal components. These paranodal changes occurred without internodal myelin damage. The distribution and pattern of paranodal disruption suggests that these changes are the direct result of mechanical stress. Electron microscopy confirmed loss of paranodal axoglial junctions.

Discussion—Our data show that chronic nerve compression disrupts paranodal junctions and axonal domains required for proper peripheral nerve function. These results provide important clues toward better understanding of the pathophysiology underlying nerve dysfunction in compression neuropathies.

Keywords

compression neuropathy; node of Ranvier; paranodal junction; axon-glia interactions; mouse model

INTRODUCTION

Peripheral nerves are often exposed to mechanical stress leading to various forms of compression neuropathies with symptoms such as weakness, altered sensation, or pain.

Address correspondence to: Keiichiro Susuki, Department of Neuroscience, Cell Biology, and Physiology, Boonshoft School of Medicine, Wright State University, 3640 Colonel Glenn Highway, Dayton, Ohio 45435, Tel: (937) 775-2292 Fax: (937) 775-3391, keiichiro.susuki@wright.edu.

*Current affiliation: Department of Molecular Neurobiology, Tokyo University of Pharmacy and Life Sciences, Hachioji, Japan

Carpal tunnel syndrome due to focal compression of the median nerve at the wrist is the most common compression neuropathy.[1] It produces focal slowing of median motor and sensory conduction velocities.[2] Median nerves in patients with mild or moderate carpal tunnel syndrome also have a greater sensitivity in response to focal nerve compression at the wrist, suggesting impaired axonal function in compressed nerves.[3] Morphological studies of human patients have revealed locally damaged myelin structures or demyelination followed by remyelination at the sites of compression.[4–6] However, the underlying pathophysiology of nerve conduction failure and altered axonal excitability in compressed nerves is not fully understood.

Myelinated nerve fibers are composed of highly polarized structures that enable rapid and efficient nerve conduction (Fig. 1A).[7] Nodes of Ranvier, short gaps between 2 adjacent myelin segments, are the functional excitable domains along myelinated axons. High densities of voltage-gated Na^+ channels clustered at these unmyelinated nodal gaps are responsible for action potential generation, whereas the majority of the axon is insulated by myelin sheaths, which facilitates internodal conduction. At paranodes flanking each side of a node, myelinating Schwann cells and the axon form junctions that play key roles for node assembly.[8] Paranodal junctions also contribute to assembly of high density clustering of the molecular complex that includes voltage-gated K^+ (Kv) channels at the the domains next to paranodes called juxtaparanodes.[9–11] Studies of the disruption of nodal molecular organization and structures after nervous system disease or injury have provided profound insights into the pathophysiology of these disorders.[12] A skin biopsy from an area innervated by the median nerve in patients with carpal tunnel syndrome displayed elongated nodes that may be an adaptive phenomenon of nerve well beyond the focal compression site.[13] However, nodal changes at the site of nerve compression have not been well studied,[14] despite the fact that some studies have shown that the cellular events related to mechanical forces alter nodal and paranodal structures.[15,16] In this study, we analyzed the molecular organization and fine structure of nodes of Ranvier at the site of compression in a mouse chronic nerve compression (CNC) model.[17]

MATERIALS AND METHODS

Mice

Female C57BL/6 mice (Envigo, Indianapolis, IN) were used for the CNC model at age 6 weeks as described elsewhere.[17] In brief, under general anesthesia with 2% isoflurane (Vedco, St. Joseph, MO), a silastic tube (inner diameter of 0.51 mm and length of 3 mm) (Cole-Palmer, Vernon Hills, IL) was placed around the left sciatic nerve in the middle of the thigh. The right sciatic nerve was isolated using the same technique without placement of tubing to serve as a sham control. For post-operative analgesia, buprenorphine (0.1 mg/kg; Reckitt Benckiser Pharmaceuticals, Richmond, VA) was given subcutaneously immediately after surgery. Carprofen (5 mg/kg; Putney, Portland, ME) was also given subcutaneously immediately after surgery and 24 hours later. Mice were housed in the Laboratory Animal Resources at Wright State University at 22°C under standard 12 hour light/12 hour dark conditions with *ad libitum* access to water and standard chow. All animal procedures were

approved by the Institutional Animal Care and Use Committee at Wright State University (protocol number: AUP1001).

Motor nerve conduction study

Conduction in motor nerve fibers connected to the plantar muscles was examined under general anesthesia with 2% isoflurane inhalation at different time points after surgery: 3 days (n=6), 1 week (n=6), and 12 weeks (n=8). Body temperature at the thigh was monitored and kept between 34 and 35°C by use of a heating pad. To stimulate the nerve, needle electrodes were inserted close to the sciatic nerve and its tibial branch at 3 levels: ankle, knee, and sciatic notch. At each level, an electrode close to the nerve acted as the cathode, and a remote subcutaneous electrode as the anode. Recording from the plantar muscles was through needle electrodes; one was placed transversely over the muscle bellies in the sole of the foot and the other was inserted subcutaneously at a distance. Supramaximal stimulations were used, and the evoked compound muscle action potentials (CMAPs) were recorded with a PowerLab signal acquisition set-up (ADInstruments, Colorado Springs, CO). Amplitude was measured between base line and negative peak of CMAPs, and duration was measured between onset and final return to the baseline. Motor nerve conduction velocity was measured between the knee and the sciatic notch.

Immunofluorescence

Tissues were prepared for immunohistochemistry at 1 week (n=3), 2 weeks (n=5), 4 weeks (n=3), and 12 weeks (n=4) after surgery. Sciatic nerves were rapidly dissected and immediately fixed in ice-cold 4% paraformaldehyde in 0.1 M phosphate buffer (PB) (pH 7.2) for 30 min. After fixation, nerves were cryoprotected with 20% sucrose in 0.1 M PB overnight at 4°C. The nerves were then frozen in Tissue Freezing Medium (Electron Microscopy Sciences, Hatfield, PA). Sections were then cut (16 μm) by cryostat (HM550, Thermo Fisher Scientific, Waltham, MA), placed in 0.1 M PB, spread on gelatin-coated coverslips, and allowed to air dry. For teased fiber preparations, sciatic nerves were transferred in 0.1 M PB (pH 7.4) after fixation. The nerves were teased apart gently and spread on gelatin-coated coverslips, and air-dried. After permeabilization in 0.1 M PB, pH 7.4 containing 0.3% Triton X-100 and 10% goat serum (PBTGS), samples were incubated overnight at 4°C with primary antibodies diluted to appropriate concentrations in PBTGS. Samples were then thoroughly rinsed in PBTGS, followed by application of fluorescently labeled secondary antibodies (1:1000 in PBTGS) for 1 hr at room temperature. Finally, labeled samples were rinsed consecutively in PBTGS, 0.1 M PB, and 0.05 M PB for 10 min each. The samples were then air-dried and mounted on slides with a mounting medium (KPL, Gaithersburg, MD). Images were captured with a fluorescence microscope (Axio Observer Z1 with Apotome 2 fitted with Axiocam Mrm CCD camera) (Carl Zeiss, Thornwood, NY). Image analyses were performed using ZEN software from Carl Zeiss. The following primary antibodies were used: mouse monoclonal antibodies against βII spectrin (BD Biosciences, San Jose, CA), ankyrinG (N106/36, UC Davis/NIH NeuroMab Facility, Davis, CA), Kv1.2 (K14/16, NeuroMab), rabbit antibodies against contactin-associated protein (Caspr), βIV spectrin (kindly provided by Dr. Matthew N. Rasband, Baylor College of Medicine, Houston, TX), gliomedin (kindly privided by Dr. Elior Peles, Weizmann Institute of Science, Rehovot, Israel), dystrophin-related protein 2 (DRP2) (kindly provided

by Dr. Peter J. Brophy, Centre for Neuroscience Research, University of Edinburgh, Edinburgh, UK); chicken antibodies to neurofascin (NF) (R&D Systems, Minneapolis, MN). Secondary antibodies were from Jackson ImmunoResearch Laboratories (West Grove, PA).

Morphological analyses

Tissues were prepared for light microscopy and electron microscopy at 2 weeks after surgery (n=4). Mice were deeply anesthetized by intraperitoneal injection of Euthasol® solution (pentobarbital sodium and phenytoin sodium, Virbac, Fort Worth, TX). Mice were then transcardially perfused with 0.1 M Millonig buffer containing 4% paraformaldehyde and 5% glutaraldehyde**,** pH 7.4. Following 2 weeks of post-fixation in the same fixative, sciatic nerves were harvested and thoroughly rinsed in 0.1 M cacodylate buffer. The nerves were postfixed in 2% osmium tetroxide solution in 0.1 M cacodylate buffer, pH 7.4, for 1 hr. After washing in 0.1 M cacodylate buffer, nerves were dehydrated through a graded ethanol series and embedded in low-viscosity resin. Cross-sections of 1 μm were cut and stained with toluidine blue. Images were captured with a microscope (Axio Observer Z1, Carl Zeiss). The light microscopy was performed in the Microscopy Core Facilities at Wright State University. Supplies and chemicals were from Electron Microscopy Sciences. Sciatic nerve samples for transmission electron microscopy (TEM) were prepared as described elsewhere.[18] Briefly, nerves were embedded in PolyBed 812 resin (PolySciences, Warrington, PA), and 90 nm sections were stained with uranyl acetate and lead citrate. Ultrathin sections were imaged using a JEOL JEM 1230 transmission electron microscope (JEOL, Peabody, MA) equipped with a Gatan Orius SC 1000 CCD camera (Gatan Inc., Pleasanton, CA).

Statistical analyses

Mann-Whitney test was used for comparison of control and nerve compression groups. Differences were considered significant at $P<0.05$. In some graphs, data are shown in box-and-whisker plot: median, a line across the box; 25th and 75th percentiles, lower and upper box edges, respectively; minimum and maximum, the values below and above the box, respectively.

RESULTS

Nerve conduction slowing at the compressed mouse sciatic nerves

To analyze changes in nodal molecular architecture due to nerve compression, we utilized a mouse model established by Gupta et al.[17] We confirmed their results as follows. Motor nerve conduction velocity across the compressed site (knee-sciatic notch segment) was comparable to that in sham control nerves 3 days after compression [median=40.1 m/s in control and 34.3 m/s in compressed nerves (n=6), $P=0.26$, Supplementary Figure]. Significant nerve conduction slowing was observed at 1 week [median=37.1 m/s in control and 29.3 m/s in compressed nerves (n=6), $P<0.01$] and 12 weeks [median=46.7 m/s in control and 33.7 m/s in compressed nerves (n=8), $p<0.01$]. No significant difference was seen in CMAP amplitudes after knee stimulation [median=13.8 mV in control and 14.0 mV in compressed nerves at 1 week (n=6), $P=0.87$; 15.5 mV in control and 15.9 mV in compressed nerves at 12 weeks (n=8), $P=0.83$], suggesting little or no axonal degeneration.

Light microscopy of cross-sections at the knee segment (distal to the compressed site; at the level of knee stimulation) showed few degenerating fibers near the surface of the nerves (Supplementary Figure). One mouse had a small cluster of ~10 degenerating fibers, but overall frequency of degeneration was very low: 0.69% (14 degenerating fibers/2040 myelinated axons); 0.11% (2/1829); or 0.14% (2/1401) (3 mice at 2 weeks were analyzed). Therefore, this mouse CNC model induced nerve conduction slowing at the compressed site of the mouse sciatic nerve with minimal degeneration of myelinated axons as described previously.[17]

Disrupted molecular organization at paranodes and juxtaparanodes in the compressed nerves

To examine the molecular organization of nodes, paranodes, and juxtaparanodes, we next performed immunofluorescence. The most striking abnormality in the compressed nerves was the presence of altered clusters of paranodal molecules. Paranodal axoglial junctions consist of a heterotrimeric cell adhesion complex composed of the glial 155 kDa isoform of NF (NF155) and an axonal complex of contactin and Caspr.[19] These paranodal junctions have been proposed to serve as a diffusion barrier that excludes juxtaparanodal proteins including voltage-gated K^+ channels such as Kv1.2.[9–11] The clusters of NF155 and Caspr were often split, and the border between the paranode and juxtaparanodal Kv1.2 cluster was moved away from the node (Fig. 1C). In most cases, the paranodal area close to the juxtaparanode was affected, whereas paranodal clusters next to the node remained intact. In some affected paranodes, the NF155 and Caspr clusters were dispersed with apparent reduction of signal intensity (Fig. 1D,E). Measurement of Caspr cluster length revealed significant elongation of the affected paranodes (Fig. 1F). In addition, we occasionally found enlargement of axons at the affected paranodes or juxtaparanodes as shown in Fig. 1E: 18 of 106 (17.0%) affected paranodes show apparent increase of Caspr and/or Kv1.2 cluster width (data were collected from 5 mice at 2 weeks after compression).

We then asked whether the border between the paranode and juxtaparanode was disrupted due to nerve compression. Despite disruption of NF155 and Caspr clusters, juxtaparanodal Kv1.2 was excluded from the paranodal area in some cases (Fig. 1C). Occasionally, juxtaparanodal Kv1.2 mislocalized to the paranodal area with dispersed and elongated NF155 and Caspr staining (Fig. 1D), indicating that the function of paranodes as a molecular barrier was lost. Especially at later time points (4 and 12 weeks), we often observed remarkably dispersed NF155 and Caspr clusters with overlapping disorganized Kv1.2 staining in the compressed nerves (Fig. 1G,H). The frequency of loss of paranode/juxtaparanode border per disrupted paranodes was significantly higher at 12 weeks (median=78.4%, 4 mice) compared to that at 2 weeks (median=56.3%, 5 mice, $P<0.05$). These findings demonstrate that chronic compression of peripheral nerves disrupts paranodal axon-glial junctions. Disrupted paranodal junctions may still restrict the mobility of juxtaparanodal components during the early stage of compression injury, but their function as a molecular barrier is lost at the advanced stage.

Disruption of nodal clusters in the compressed nerves

In addition to their function to exclude juxtaparanodal components, paranodal axoglial junctions are proposed to act as a barrier to restrict the mobility of nodal proteins, thereby contributing to the assembly of nodes of Ranvier.[8,20] Therefore, we next examined whether nodal clusters were disrupted due to peripheral nerve compression. The cell adhesion molecule186-kDa isoform of NF (NF186) is highly enriched at nodal axolemma,[21] and plays a key role in nodal assembly and maintenance.[22,23] Despite the paranodal disruption demonstrated by altered NF155 and Caspr staining, nodal clusters were mostly preserved (Fig. 1C–E,G). However, we occasionaly found disorganized nodal clusters which were always associated with remarkably disrupted paranodes (Fig. 2B). Nodal disruption was relatively rare: at 1 week from compression, among 65 nodes with disrupted NF, Caspr, or Kv1.2 clusters, only 4 (6.2%) nodes were disrupted (data were collected from 3 mice). Similarly, the frequency of nodal disruption was: 11 of 93 (11.8%) at 2 weeks (5 mice); 4 of 67 (6.0%) at 4 weeks (3 mice); and 13 of 148 (8.8%) at 12 weeks (4 mice).

In addition to the paranodal junctions, glial contact mediated by nodal extracellular matrix protein such as gliomedin plays a key role in peripheral nerve node assembly and maintenance.[8,24,25] At the affected nodes in the compressed nerves, we found the clusters of gliomedin were disrupted but partially overlapped with altered clusters of NF and ankyrinG (Fig. 2D). Ankyrin G is a scaffolding protein that binds with both NF186 and Na^+ channels at the nodal axons.[26] In contrast, at the nodes associated with mildly disrupted paranodes, gliomedin clusters were preserved (Fig. 2E). Similarly, the clusters of βIV spectrin that link the Na^+ channel-NF186-ankyrinG complex to the actin cytoskeleton at nodal axons[27] were also altered at the affected nodes (Fig. 2G). Thus, node of Ranvier damage in the compressed nerves was associated with disruption of all mechanisms that ensure nodal protein complex assembly and maintenance.

Next, we examined the evidence of early nodal clustering in remyelinating axons. Nodal proteins are associated with the edges of myelinating Schwann cells in nerves during remyelination,[28] a characteristic finding called a heminode. Heminodes were observed in the compressed nerves (Fig. 2H), but were rare at all time points. At 1 week from compression, among 65 nodes with disrupted NF, Caspr, or Kv1.2 clusters, only 1 (1.5%) showed heminodal NF clusters (data were collected from 3 mice). Similarly, the frequency of heminodes was: 2 of 93 (2.2%) at 2 weeks (5 mice); 1 of 67 (1.5%) at 4 weeks (3 mice); and 2 of 148 (1.4%) at 12 weeks (4 mice). These findings show that chronic mechanical stress causes sustained disruption followed by re-formation of nodes of Ranvier, although they are relatively rare.

Paranodal disruption occurs without internodal myelin damage

Peripheral nerve compression results in thinner myelin, shortened internodal length, and disorganized Schwann cell architecture on the myelin outer surface.[17] On the outer surface of internodal myelin, longitudinal and transverse bands of Schwann cell cytoplasm are formed (Fig. 3A).[29,30] These structures permit Schwann cells to lengthen in response to axonal growth to ensure rapid nerve impulse transmission.[29] We confirmed the results described in the previous study:[17] Schwann cell cytoplasmic bands were disorganized, and

immunostaining of DRP2 was reduced in some myelin sheaths in the compressed nerves at 2 weeks after surgery (Fig. 3B). Molecular organization of nodes and paranodes is disrupted during acute demyelination in the peripheral nervous system.[31] To determine whether the paranodal and nodal disruption described above (Fig. 1,2) is secondary to myelin sheath damage, we immunostained teased nerve fibers with myelin and nodal markers. The signal intensity and characteristic cobble stone-like pattern of DRP2 immunostaining was preserved in 35 of 47 (74.5%) myelin sheaths associated with disorganized NF155 and Kv1.2 staining (Fig. 3C) (data were collected from 3 mice at 2 weeks).

We also examined axoglial interactions in internodal segments. In normal peripheral nerves, juxtaparanodal proteins such as Kv1.2 are concentrated throughout the internodes in a double strand that flanks paranodal junction components axonal Caspr and Schwann cell NF155, and apposes the inner mesaxon of the myelin sheath (Fig. 3D).[32,33] In the compressed nerves at 2 weeks, this characteristic spiral strand shape of immunostaining mostly disappeared at the area of disorganized NF155, Caspr, and Kv1.2 staining, but was still preserved in the internode (Fig. 2E,3E), suggesting that axoglial interactions remain intact except for the paranodal area. We observed a spiral strand shape of Caspr and Kv1.2 immunostaining in 78 of 80 (97.5%) internodal segments near juxtaparanodes in control nerves; 79 of 80 (98.8%) segments associated with intact paranodes in the compressed nerves; and 56 of 63 (88.9%) segments associated with disrupted paranodes in the compressed nerves (data were collected from 4 mice at 2 weeks). These findings demonstrate that the nerve compression can disrupt paranodes without damage to internodal myelin sheaths.

Distribution of paranodal and nodal alterations in the compressed nerves

The paranodal and nodal alterations described above (Fig. 1–3) showed characteristic distribution in the compressed nerves. These abnormalities were not uniformly present but were highly concentrated at the regions near both edges of the compressed site (Fig. 4A). The striking feature of the paranodal disruption was its laterality. More than 70% showed disrupted paranodes on the side further from the center of compressed site (lateral side) whereas the other side remained intact (80.5% at 2 weeks and 71.4% at 12 weeks; Fig. 4A,B). Disrupted paranodes were rarely seen in the middle of the compressed site: 16 of 346 (4.6%) nodes were associated with disrupted Caspr and Kv1.2 clusters at 2 weeks (data were collected from 4 mice). In contrast, the area near the edge of the tube had a much higher frequency of disrupted paranodes and nodes (Fig. 4C; median=20.3%, 4 mice). The nodal/paranodal disruption tended to increase at 12 weeks (Fig. 4C; median=50.4%, 4 mice), although the difference did not reach statistical significance. These results suggest that the paranodal and nodal alterations are more likely to be the direct result of mechanical stress caused by the tubing placed around the nerves.

Disruption of paranodal fine structures

To further examine the disrupted paranodal structures, we performed TEM using longitudinal sections of sciatic nerves at 2 weeks (4 mice). The most striking feature in the compressed nerves was the loss of paranodal axoglial junctions. Paranodal junctions are characterized by intercellular transverse bands, regularly arrayed densities between the

axolemma and lateral loops of myelin (Fig. 5A,B).[9–11,34,35] We found that the transverse bands were lost in some paranodal lateral loops (predominantly in inner loops close to the juxtaparanodes) in the compressed nerves (Fig. 5E,G). We also found remote paranodal lateral loops located away from nodes (Fig. 5C,J, arrows). These paranodal changes correspond well to the reduced and elongated NF155 and Caspr staining shown in Fig. 1C,D. We also found focal enlargement of axons with abnormal accumulation of mitochondria at the affected paranodal or juxtaparanodal area (Fig. 5F,H,I), suggesting impaired axonal transport. This abnormal mitochondrial accumulation is consistent with the axon swelling demonstrated by Caspr and/or Kv1.2 staining in immunofluorescence (Fig. 1E). These paranodal changes were often associated with preserved myelin lamellae (Fig. 5C,D,F), further supporting the observation that paranodal disruption occurred without internodal myelin damage (Fig. 3). We also confirmed asymmetrical paranodal disruption described in Fig. 4. The paranode on the right in Fig. 5J has thin myelin which tapers towards the node. Similar to the previous observation in guinea-pig nerve compression,[36] several myelin loops were observed remote from the node (Fig. 5J, inset, arrows). These ectopic lateral loops can be a deformity caused by mechanical stress, presumably leading to thinner compact myelin near the disrupted paranode.[36] We also found thin myelin sheaths, consistent with demyelination followed by remyelination (data not shown). Finally, we observed no axonal degeneration, consistent with preserved CMAP amplitudes and few degenerating fibers observed in light microscopy (Supplementary Figure). These ultrastructural analyses provide further evidence that axoglial interactions at paranodes are disrupted by chronic peripheral nerve compression.

DISCUSSION

Using the disease model of compression neuropathies, we show that chronic mechanical stress to the peripheral nerves disrupts paranodal axoglial junctions. These paranodal changes lead to disruption of functional domains, nodes of Ranvier, and juxtaparanodes, which are required for rapid and efficient propagation of action potentials along the myelinated axons.

Paranodal axoglial junctions are formed by a heterotrimeric cell adhesion complex consisting of the glial NF155 and an axonal complex of contactin and Caspr.[19] In the compressed nerves, this paranodal cell adhesion complex was remarkably dispersed and was often associated with mislocalization of juxtaparanodal Kv1.2 to the paranodal area (Fig. 1). This was further confirmed by loss of paranodal transverse bands by TEM (Fig. 5). These changes in the compressed nerves are consistent with previous observations that showed the roles of this cell adhesion complex in formation and maintenance of paranodal axoglial junctions and juxtaparanodal components. Mutant mice lacking Caspr,[9] contactin,[10] or NF155[11] show: i) loss of a paranodal Caspr-contactin-NF155 complex; ii) mislocalization of juxtaparanodal components to the paranodal region immediately adjacent to nodes; iii) loss of transverse bands; and iv) nerve conduction slowing in sciatic nerves. Ablation of NF155 in adult myelinating glia revealed gradual loss of paranodal axoglial junctions and mislocalization of Kv channels toward nodal region in sciatic nerves.[11]

This paranodal cell adhesion complex also contributes to axonal integrity. In mutant mice lacking Caspr[37] or NF155,[11] axonal swellings accompanied by cytoskeletal disorganization and accumulation of cell organelles were frequently formed within or in close proximity to the paranodal region in cerebellar Pukinje axons. Similarly, at and near the affected paranodes in compressed nerves, we occasionally found abnormal axon swellings in immunofluorescence (Fig. 1E) and focal axon enlargement with abnormal accumulation of mitochondria on TEM (Fig. 5FH,I), consistent with impaired axonal transport. Importantly, these paranodal changes during nerve compression were mostly associated with myelin sheaths with intact internodal structures (Fig. 3) or preserved compact myelin (Fig. 5), suggesting that the paranodes are particularly vulnerable to mechanical stress.

Compared to the juxtaparanodal disorganization, nodal disruptions were rarely seen in the compressed nerves (Fig. 2). This is presumably due to preserved paranodal junctions immediately next to the nodes, whereas dispersed NF155 and Caspr clusters or loss of paranodal transverse bands were frequently seen at the area near juxtaparanodes (Fig. 1,5). Furthermore, multiple redundant mechanisms ensure node assembly, including restriction of nodal proteins by paranodal junctions, clustering of NF186 by glia-derived molecules in the extracellular matrix surrounding nodes, and stabilization of nodal proteins by axonal cytoskeletal scaffolds.[38] Indeed, even with complete loss of paranodal junctions, nodes are still formed.[9–11] However, double mutant mice with loss of Caspr and gliomedin showed altered or reduced nodal Na^+ channel clusters and nerve conduction slowing in sciatic nerves.[8] In the compressed nerves, nodes of Ranvier were disrupted when the paranodal clusters immediately next to nodes were reduced, and gliomedin and βIV spectrin clusters were concurrently disrupted.

What are the functional consequences of these paranodal alterations in the compressed nerves? Mutant mice with complete loss of paranodal junctions show remarkable nerve conduction slowing.[9–11] Compared to these mutant mice, paranodal changes in compressed nerves remain partial (Fig. 1,5). However, a mathematical model showed that even subtle retraction and partial detachment of paranodal myelin slows nerve conduction velocity.[39] Thus, it is conceivable that the disruption of paranodal junctions shown in this study causes nerve conduction slowing. Furthermore, alteration of juxtaparanodal Kv channels may affect axonal excitability. For example, in patients with amyotrophic lateral sclerosis, loss of juxtaparanodal Kv1.2 may underlie abnormally increased excitability of motor axons, thereby generating fasciculations.[40] Reduction of Kv1.2 clustering at juxtaparanodes contributes to peripheral nerve hyperexcitability in mouse model of type 2 diabetes mellitus.[41] Although the functional consequence of remarkably dispersed juxtaparanodal Kv channels towards internodes (Fig. 1G) is unclear, these changes may contribute to increased sensitivity of axons in response to focal nerve compression at the wrist in patients with mild or moderate carpal tunnel syndrome.[3] Thus, altered molecular organization at and near nodes described in this study provides important clues to better understand the pathophysiology underlying nerve dysfunction in compression neuropathies.

A previous report of the same mouse CNC model[17] showed shortened internodal length and thinner myelin sheaths, both of which cause decreased conduction velocity.[29,42] Internodal length remained shortened throughout the 12-week time course.[17] The authors proposed that

the continued presence of mechanical stimuli results in equilibrium between the opposing processes of demyelination and remyelination.[17] Consistent with this idea, we observed both disrupted nodal clusters (Fig 2B,D,G) and node re-formation (heminode, Fig 2H) throughout the 12-week time course. These nodal changes were rare, presumably due to relatively mild but continuous mechanical stress in this model. In addition, these nodal changes are observed during a limited period in the process of demyelination followed by remyelination. Disrupted paranodes tended to be more frequent at 12 weeks compared to 2 weeks (Fig 4C). In contrast, cytoplasmic bands on the outer surface of myelinating Schwann cells were disrupted at 2 weeks (as shown in Fig 3B), but were reconstituted by 12 weeks.[17] These myelin and nodal changes all contribute to the observed plateau of nerve conduction slowing in this CNC model (Supplementary Figure).[17]

Our results further confirmed previous morphological studies in compression neuropathies. In chronic median nerve compression in the guinea pig, the characteristic early change preceding demyelination consisted of a polarized distortion of the myelin sheaths, which became bulbous at 1 paranode and tapered at the other.[36,43] These changes were observed at sites both proximal and distal to the entrapment but with reversed polarity. For example, at the site distal to the entrapment, the bulbous paranodes were seen on the distal side of the myelin sheaths, and the tapered paranodes were proximal. Therefore, nodes of Ranvier are associated with bulbous paranodes on the side close to the entrapment site, and the tapered paranodes are on the other side.[36] This is consistent with our results of asymmetrical paranodal disruption (Fig. 4A,B); more than 70% showed preserved paranodal junctions on the side close to the center of the compression site (medial side), while the other side (lateral side) had dispersed and elongated Caspr and Kv1.2 clusters (tapered paranodes in TEM). Similar changes in paranodal myelin were observed in the sub-clinical entrapment of median nerves at the wrist and ulnar nerves at the elbow from human subjects[4] and an ulnar nerve at the elbow from a patient with ulnar neuropathy.[5] This characteristic pattern and distribution of paranodal disruption is considered to be due to mechanical factors caused by repetitive to and fro sliding of nerve trunks at the site of compression,[14,36] although ischemic factors[44] may have additional roles for vulnerability of paranodal junctions. Thus, our results further demonstrate that this mouse CNC model[17] recapitulates pathological features of human compression neuropathies and thereby provides a suitable tool for further research into the pathophysiology of compression neuropathies.

The paranodal and nodal disruption we have described should be mostly due to Schwann cell changes but not from the axonal side, because there is very little axonal degeneration (Supplementary Figure).[17] Myelinating Schwann cells have been considered to be the primary mediators of the disease process in compression neuropathies.[45] Current knowledge of Schwann cell responses to mechanical stress is limited. For example, an *in vitro* study suggests that the integrin signaling pathway mediates Schwann cell changes underlying compression neuropathies.[46] Downregulation of desert hedgehog, a signaling molecule produced by Schwann cells that regulates myelination, is involved in the pathogenesis of demyelination in compression neuropathies.[47] Our results demonstrate disruption of distinct domains along myelinated axons required for nerve conduction and provide more insight into the pathophysiology underlying nerve conduction failure in compression neuropathies. However, the molecular and cellular mechanisms of disruption, regeneration, or remodeling

of myelin sheaths and nodes of Ranvier in compression neuropathies remain unknown. Further studies of Schwann cell pathophysiology focusing on these structures and domains in myelinated axons are required to better understand the mechanisms of compression neuropathies and to determine therapeutic targets for novel nerve-specific approaches to improve treatment outcomes in patients with compression neuropathies.

Supplementary Material

Refer to Web version on PubMed Central for supplementary material.

Acknowledgments

This work was supported by Veterans Affairs Merit Grant (5IO1BX002565 to J.L.D.) and the National Institutes of Health (NIH)-National Institute of Neurological Disorders and Stroke Center Core Grant 5P30 NS047463. The authors thank Hanna M. Gabriel (Microscopy Core Facilities, Wright State University) for technical assiscance, and Dr. Mark M. Rich (Wright State University) for critical reading. The authors declare no competing financial interests.

Abbreviations

Caspr	contactin-associated protein
CMAP	compound muscle action potential
CNC	chronic nerve compression
DRP2	dystrophin-related protein 2
Kv	voltage-gated K^+ channel
NF	neurofascin
PB	phosphate buffer
PBTGS	phosphate buffer containing Triton X-100 and goat serum
TEM	transmission electron microscopy

References

1. Newington L, Harris EC, Walker-Bone K. Carpal tunnel syndrome and work. Best Pract Res Clin Rheumatol. 2015; 29:440–453. [PubMed: 26612240]
2. Jablecki CK, Andary MT, Floeter MK, Miller RG, Quartly CA, Vennix MJ, et al. Practice parameter: Electrodiagnostic studies in carpal tunnel syndrome. Report of the American Association of Electrodiagnostic Medicine, American Academy of Neurology, and the American Academy of Physical Medicine and Rehabilitation. Neurology. 2002; 58:1589–1592. [PubMed: 12058083]
3. Han SE, Lin CS, Boland RA, Kiernan MC. Nerve compression, membrane excitability, and symptoms of carpal tunnel syndrome. Muscle Nerve. 2011; 44:402–409. [PubMed: 21996801]
4. Neary D, Ochoa J, Gilliatt RW. Sub-clinical entrapment neuropathy in man. J Neurol Sci. 1975; 24:283–298. [PubMed: 1117305]
5. Neary D, Eames RA. The pathology of ulnar nerve compression in men. Neuropathol Appl Neurobiol. 1975; 1:69–88.
6. Mackinnon SE, Dellon AL, Hudson AR, Hunter DA. Chronic human nerve compression-a histological assessment. Neuropathol Appl Neurobiol. 1986; 12:547–565. [PubMed: 3561691]

7. Rasband MN, Peles E. The nodes of Ranvier: molecular assembly and maintenance. Cold Spring Harb Perspect Biol. 2015; 8:a020495. [PubMed: 26354894]
8. Feinberg K, Eshed-Eisenbach Y, Frechter S, Amor V, Salomon D, Sabanay H, et al. A glial signal consisting of gliomedin and NrCAM clusters axonal Na^+ channels during the formation of nodes of Ranvier. Neuron. 2010; 65:490–502. [PubMed: 20188654]
9. Bhat MA, Rios JC, Lu Y, Garcia-Fresco GP, Ching W, St Martin M, et al. Axon-glia interactions and the domain organization of myelinated axons requires neurexin IV/Caspr/Paranodin. Neuron. 2001; 30:369–383. [PubMed: 11395000]
10. Boyle ME, Berglund EO, Murai KK, Weber L, Peles E, Ranscht B. Contactin orchestrates assembly of the septate-like junctions at the paranode in myelinated peripheral nerve. Neuron. 2001; 30:385–397. [PubMed: 11395001]
11. Pillai AM, Thaxton C, Pribisko AL, Cheng JG, Dupree JL, Bhat MA. Spatiotemporal ablation of myelinating glia-specific *neurofascin* (*Nfasc*^{NF155}) in mice reveals gradual loss of paranodal axoglial junctions and concomitant disorganization of axonal domains. J Neurosci Res. 2009; 87:1773–1793. [PubMed: 19185024]
12. Susuki K. Node of Ranvier disruption as a cause of neurological diseases. ASN Neuro. 2013; 5:e00118. [PubMed: 23834220]
13. Schmid AB, Bland JD, Bhat MA, Bennett DL. The relationship of nerve fibre pathology to sensory function in entrapment neuropathy. Brain. 2014; 137:3186–3199. [PubMed: 25348629]
14. Ochoa JL. Genesis of the structural pathology of myelinated fibers in median nerve entrapment. Muscle Nerve. 2012; 46:978. Reply: Gupta R, Mozaffar T Muscle Nerve 2012, 46, 979. [PubMed: 23225392]
15. Ochoa J, Danta G, Fowler TJ, Gilliatt RW. Nature of the nerve lesion caused by a pneumatic tourniquet. Nature. 1971; 233:265–266. [PubMed: 4999642]
16. Dyck PJ, Lais AC, Giannini C, Engelstad JK. Structural alterations of nerve during cuff compression. Proc Natl Acad Sci U S A. 1990; 87:9828–9832. [PubMed: 2263633]
17. Gupta R, Nassiri N, Hazel A, Bathen M, Mozaffar T. Chronic nerve compression alters Schwann cell myelin architecture in a murine model. Muscle Nerve. 2012; 45:231–241. [PubMed: 22246880]
18. Marcus J, Honigbaum S, Shroff S, Honke K, Rosenbluth J, Dupree JL. Sulfatide is essential for the maintenance of CNS myelin and axon structure. Glia. 2006; 53:372–381. [PubMed: 16288467]
19. Charles P, Tait S, Faivre-Sarrailh C, Barbin G, Gunn-Moore F, Denisenko-Nehrbass N, et al. Neurofascin is a glial receptor for the paranodin/Caspr-contactin axonal complex at the axoglial junction. Curr Biol. 2002; 12:217–220. [PubMed: 11839274]
20. Rasband MN, Peles E, Trimmer JS, Levinson SR, Lux SE, Shrager P. Dependence of nodal sodium channel clustering on paranodal axoglial contact in the developing CNS. J Neurosci. 1999; 19:7516–7528. [PubMed: 10460258]
21. Davis JQ, Lambert S, Bennett V. Molecular composition of the node of Ranvier: identification of ankyrin-binding cell adhesion molecules neurofascin (mucin+/third FNIII domain-) and NrCAM at nodal axon segments. J Cell Biol. 1996; 135:1355–1367. [PubMed: 8947556]
22. Sherman DL, Tait S, Melrose S, Johnson R, Zonta B, Court FA, et al. Neurofascins are required to establish axonal domains for saltatory conduction. Neuron. 2005; 48:737–742. [PubMed: 16337912]
23. Desmazieres A, Zonta B, Zhang A, Wu LM, Sherman DL, Brophy PJ. Differential stability of PNS and CNS nodal complexes when neuronal neurofascin is lost. J Neurosci. 2014; 34:5083–5088. [PubMed: 24719087]
24. Eshed Y, Feinberg K, Poliak S, Sabanay H, Sarig-Nadir O, Spiegel I, et al. Gliomedin mediates Schwann cell-axon interaction and the molecular assembly of the nodes of Ranvier. Neuron. 2005; 47:215–229. [PubMed: 16039564]
25. Amor V, Feinberg K, Eshed-Eisenbach Y, Vainshtein A, Frechter S, Grumet M, et al. Long-term maintenance of Na^+ channels at nodes of Ranvier depends on glial contact mediated by gliomedin and NrCAM. J Neurosci. 2014; 34:5089–5098. [PubMed: 24719088]

26. Kordeli E, Lambert S, Bennett V, Ankyrin G. A new ankyrin gene with neural-specific isoforms localized at the axonal initial segment and node of Ranvier. J Biol Chem. 1995; 270:2352–2359. [PubMed: 7836469]
27. Berghs S, Aggujaro D, Dirkx R Jr, Maksimova E, Stabach P, Hermel JM, et al. βIV spectrin, a new spectrin localized at axon initial segments and nodes of Ranvier in the central and peripheral nervous system. J Cell Biol. 2000; 151:985–1002. [PubMed: 11086001]
28. Dugandzija-Novaković S, Koszowski AG, Levinson SR, Shrager P. Clustering of Na^+ channels and node of Ranvier formation in remyelinating axons. J Neurosci. 1995; 15:492–503. [PubMed: 7823157]
29. Court FA, Sherman DL, Pratt T, Garry EM, Ribchester RR, Cottrell DF, et al. Restricted growth of Schwann cells lacking Cajal bands slows conduction in myelinated nerves. Nature. 2004; 431:191–195. [PubMed: 15356632]
30. Susuki K, Raphael AR, Ogawa Y, Stankewich MC, Peles E, Talbot WS, et al. Schwann cell spectrins modulate peripheral nerve myelination. Proc Natl Acad Sci USA. 2011; 108:8009–8014. [PubMed: 21518878]
31. Arroyo EJ, Sirkowski EE, Chitale R, Scherer SS. Acute demyelination disrupts the molecular organization of peripheral nervous system nodes. J Comp Neurol. 2004; 479:424–434. [PubMed: 15514980]
32. Arroyo EJ, Xu YT, Zhou L, Messing A, Peles E, Chiu SY, et al. Myelinating Schwann cells determine the internodal localization of Kv1.1, Kv1. 2, Kvbeta2, and Caspr. J Neurocytol. 1999; 28:333–347. [PubMed: 10739575]
33. Ivanovic A, Horresh I, Golan N, Spiegel I, Sabanay H, Frechter S, et al. The cytoskeletal adapter protein 4.1G organizes the internodes in peripheral myelinated nerves. J Cell Biol. 2012; 196:337–344. [PubMed: 22291039]
34. Dupree JL, Coetzee T, Blight A, Suzuki K, Popko B. Myelin galactolipids are essential for proper node of Ranvier formation in the CNS. J Neurosci. 1998; 18:1642–1649. [PubMed: 9464989]
35. Rosenbluth J. Multiple functions of the paranodal junction of myelinated nerve fibers. J Neurosci Res. 2009; 87:3250–3258. [PubMed: 19224642]
36. Ochoa J, Marotte L. Nature of the nerve lesion caused by chronic entrapment in the guinea-pig. J Neurol Sci. 1973; 19:491–495. [PubMed: 4724822]
37. Garcia-Fresco GP, Sousa AD, Pillai AM, Moy SS, Crawley JN, Tessarollo L, et al. Disruption of axo-glial junctions causes cytoskeletal disorganization and degeneration of Purkinje neuron axons. Proc Natl Acad Sci U S A. 2006; 103:5137–5142. [PubMed: 16551741]
38. Susuki K, Chang KJ, Zollinger DR, Liu Y, Ogawa Y, Eshed-Eisenbach Y, et al. Three mechanisms assemble central nervous system nodes of Ranvier. Neuron. 2013; 78:469–482. [PubMed: 23664614]
39. Babbs CF, Shi R. Subtle paranodal injury slows impulse conduction in a mathematical model of myelinated axons. PLoS One. 2013; 8:e67767. [PubMed: 23844090]
40. Shibuya K, Misawa S, Arai K, Nakata M, Kanai K, Yoshiyama Y, et al. Markedly reduced axonal potassium channel expression in human sporadic amyotrophic lateral sclerosis: an immunohistochemical study. Exp Neurol. 2011; 232:149–153. [PubMed: 21906595]
41. Zenker J, Poirot O, de Preux Charles AS, Arnaud E, Médard JJ, Lacroix C, et al. Altered distribution of juxtaparanodal Kv1.2 subunits mediates peripheral nerve hyperexcitability in type 2 diabetes mellitus. J Neurosci. 2012; 32:7493–7498. [PubMed: 22649228]
42. Waxman SG. Determinants of conduction velocity in myelinated nerve fibers. Muscle Nerve. 1980; 3:141–150. [PubMed: 6245357]
43. Anderson MH, Fullerton PM, Gilliatt RW, Hern JE. Changes in the forearm associated with median nerve compression at the wrist in the guinea-pig. J Neurol Neurosurg Psychiatry. 1970; 33:70–79. [PubMed: 4313856]
44. Jung J, Hahn P, Choi B, Mozaffar T, Gupta R. Early surgical decompression restores neurovascular blood flow and ischemic parameters in an in vivo animal model of nerve compression injury. J Bone Joint Surg Am. 2014; 96:897–906. [PubMed: 24897737]
45. Gupta R, Steward O. Chronic nerve compression induces concurrent apoptosis and proliferation of Schwann cells. J Comp Neurol. 2003; 461:174–186. [PubMed: 12724836]

46. Lin MY, Frieboes LS, Forootan M, Palispis WA, Mozaffar T, Jafari M, et al. Biophysical stimulation induces demyelination via an integrin-dependent mechanism. Ann Neurol. 2012; 72:112–123. [PubMed: 22829273]

47. Jung J, Frump D, Su J, Wang W, Mozaffar T, Gupta R. Desert hedgehog is a mediator of demyelination in compression neuropathies. Exp Neurol. 2015; 271:84–94. [PubMed: 25936873]

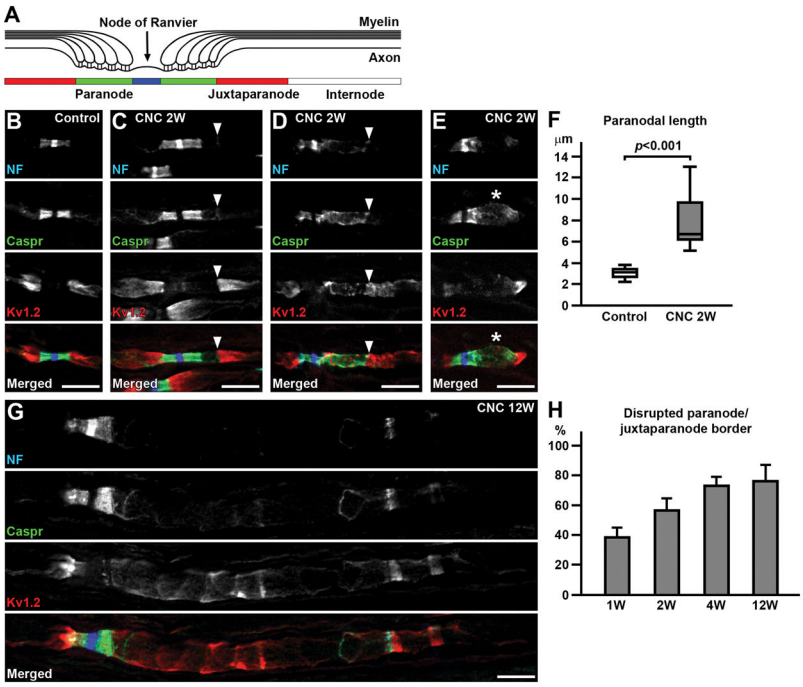

FIGURE 1.

Disrupted molecular organization at paranodes and juxtaparanodes. **(A)** Polarized domains along myelinated axons. **(B–E)** Sections of control **(B)** or compressed nerves (CNC, 2 weeks) **(C–E)** immunostained for neurofascin (NF) in blue (strong staining of NF186 at nodal axolemma and weak staining of NF155 at paranodal glia), Caspr in green, and Kv1.2 in red. **(C)** Disrupted paranode (right side of the node) but no Kv1.2 mislocalization. Note thin NF155 and Caspr staining at the paranode/juxtaparanode border (arrowhead). **(D)** Disrupted paranode (right side of the node) with overlaping Kv1.2. Arrowhead indicates the edge of paranodal clusters. **(E)** Disrupted paranode with enlarged axon (asterisk). **(F)** Length of Caspr staining (n=16, control; n=17, CNC at 2 weeks, from 4 mice). **(G)** Disrupted paranode (right side of the node) with remarkably dispersed NF155 and Caspr clusters and disorganized Kv1.2 staining in the compressed nerve at 12 weeks. **(H)** Frequency of disrupted paranode/juxtaparanode border (as depicted in D and G) per altered paranodes. Data were collected from 3 mice at 1 week, 5 mice at 2 weeks, 3 mice at 4 weeks, and 4 mice at 12 weeks. Mean and standard deviation (error bars) are shown. Scale bars = 10 µm **(B–E,G)**.

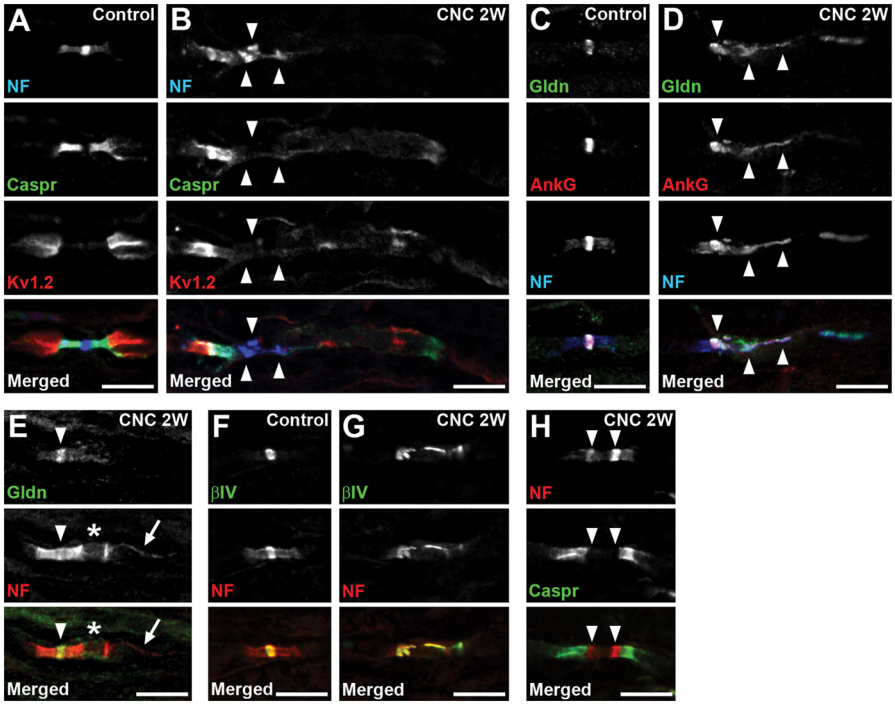

FIGURE 2.

Disrupted molecular organization at nodes. **(A,B)** Sections of control **(A)** or compressed nerves (CNC, 2 weeks) **(B)** are immunostained as indicated. **(B)** Neurofascin (NF) and Caspr staining on the right side of the nodes are remarkably reduced and dispersed. Arrowheads indicate disrupted clusters of NF. **(C,D)** Sections of control **(C)** or compressed nerves (2 weeks) **(D)** are immunostained for gliomedin (Gldn) in green, ankyrinG (AnkG) in red, and NF in blue. **(D)** Gliomedin and NF are partially co-localized with disorganized nodal ankyrinG clusters (arrowheads). **(E)** Section of compressed nerve (2 weeks) is immunostained for gliomedin in green and NF in red. The paranode on the right side of the node is disrupted (asterisk), whereas the gliomedin cluster is preserved (arrowhead). Arrow indicates NF155 enriched at inner mesaxon of the myelin. **(F,G)** Sections of control **(F)** or compressed nerves (2 weeks) **(G)** are immunostained for βIV spectrin (βIV) in green, and NF in red. **(G)** Clusters of both βIV spectrin and NF are disorganized. **(H)** Section of compressed nerve (2 weeks) is immunostained for NF in red and Caspr in green. Arrowheads indicate heminodal NF clusters that are present very close. Scale bars = 10 μm **(A–H)**.

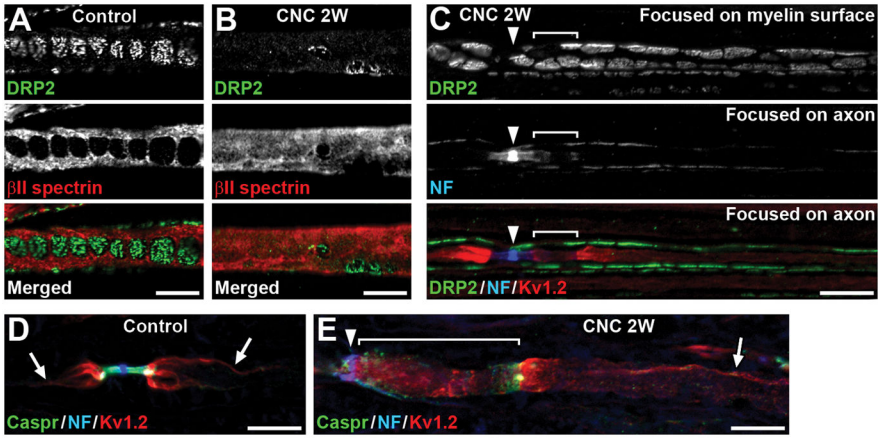

FIGURE 3.

Paranodal disruption can occur without myelin damage in internodes. **(A,B)** Teased fibers of control **(A)** or compressed nerves (CNC, 2 weeks) **(B)** are immunostained for dystrophin-related protein 2 (DRP2) (green) and βII spectrin (red). **(B)** DRP2 immunostaining is remarkably reduced, and βII spectrin staining is diffusely present. **(C)** Teased fiber of compressed nerve (2 weeks) is immunostained for DRP2 (green), NF (blue), and Kv1.2 (red). Arrowhead indicates node of Ranvier. Top panel shows DRP2 staining focused on the outer surface of myelin sheath. Middle and bottom panels are focused on the axon. NF staining is dispersed and elongated at the paranode on the right side of the node with partial overlap of Kv1.2 staining (bracket). Note the characteristic cobble stone-like pattern of DRP2 staining is preserved. **(D,E)** Sections of control **(D)** or compressed nerves (2 weeks) **(E)** are immunostained for Caspr (green), NF (blue), and Kv1.2 (red). Arrows indicate Kv1.2 enriched at the axolemma where it apposes the inner mesaxon of the myelin sheath. **(E)** Kv1.2 staining in internode is preserved (arrow), whereas paranode is remarkably elongated and disorganized with Kv1.2 mislocalization (bracket). Arrowhead indicates node of Ranvier. Scale bars = 10 μm **(A–E)**.

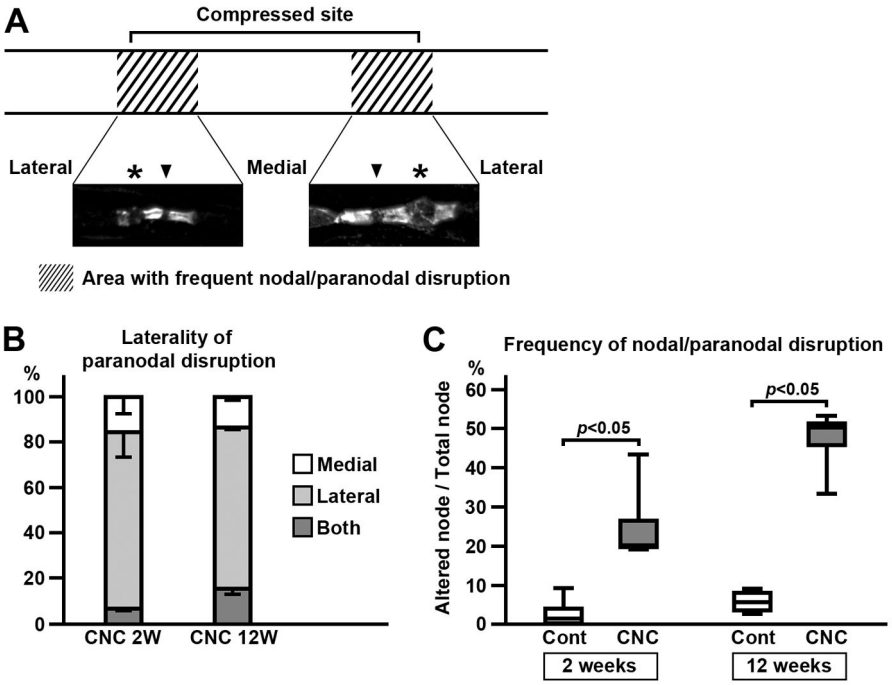

FIGURE 4.

Distribution of paranodal disruption in compressed nerves. **(A)** Altered paranodes or nodes were frequently observed in the area near both edges of compressed site and in a short segment outside of the tubing (shaded areas). Representative images of Caspr immunostaining in the compressed nerve (2 weeks) are shown. Paranode on lateral side (far from the center of compressed site) is more frequently disrupted (asterisks) than the medial side (close to the center of compressed site). Arrowheads indicate nodes. **(B)** Laterality of paranodal disruption. One NF cluster with Caspr and Kv1.2 staining on both sides is counted as 1 node. At both 2 weeks (4 mice) and 12 weeks (4 mice), nodes with disrupted paranodes on lateral sides are predominant. Mean and standard deviation (error bars in the boxes) are shown. **(C)** Frequency of paranodal and nodal disruption at the area where the abnormalities are most abundant (shaded area in panel A). One NF cluster with Caspr and Kv1.2 staining on both sides is counted as 1 node. Node is considered to be altered when 1 or more of these clusters were disrupted. Data were obtained from 4 mice at 2 weeks and 4 mice at 12 weeks.

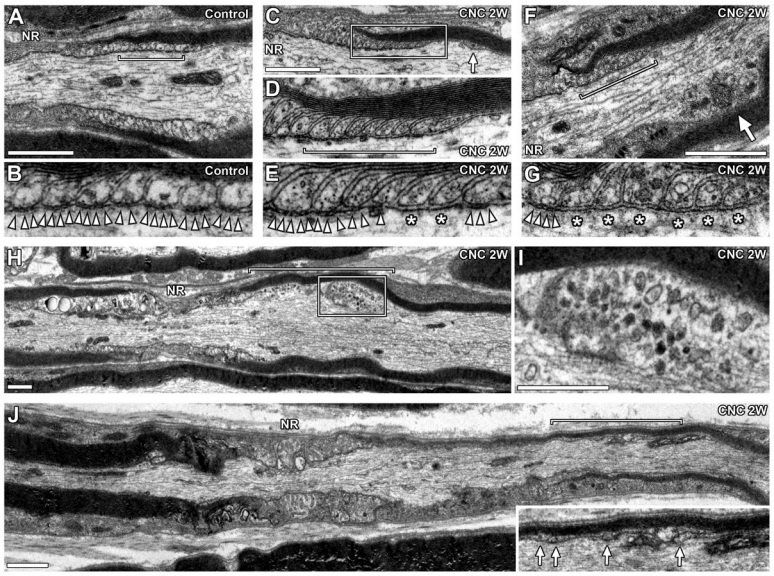

FIGURE 5.

Disrupted paranodal fine structures. TEM images of longitudinal sections of compressed nerves (2 weeks). **(A)** Normal paranode. **(B)** Enlarged image of the designated area in panel A (bracket) showing transverse bands (arrowheads). **(C)** Paranode in compressed nerve. Arrow indicates remote lateral loop. **(D)** Enlarged image of the boxed area in panel C. Myelin lamellae and lateral loops are preserved. **(E)** Enlarged image of lateral loops at the designated area in panel D (bracket). Transverse bands (arrowheads) are absent in two lateral loops (asterisks). **(F)** Paranode in compressed nerve. Arrow indicates enlarged axon with abnormal mitochondria accumulation. **(G)** Enlarged image of lateral loops in the designated area of panel F (bracket). Transverse bands (arrowheads) are absent in 6 innermost lateral loops (asterisks). **(H)** Focal axon enlargement in compressed nerve (bracket). **(I)** Enlarged image of the boxed area in panel H. Abnormal mitochondria accumulation. **(J)** Myelinated axon in compressed nerve. Paranode on the right side of the node is remarkably disorganized. Inset is an enlarged image of designated area (bracket) showing remote lateral loops (arrows). Myelin sheath on the right side is thinner than the left side. NR indicates location of node of Ranvier **(A,C,F,H,J)**. Scale bars = 1 μm **(A,C,F,H,I,J)**.